Influence of Ge content on the optical properties of *X* and *W* centers in dilute Si-Ge alloys

J. P. Leitão,[1,*] A. Carvalho,[1] J. Coutinho,[1] R. N. Pereira,[1] N. M. Santos,[1] A. O. Ankiewicz,[1] N. A. Sobolev,[1] M. Barroso,[1] J. Lundsgaard Hansen,[2] A. Nylandsted Larsen,[2] and P. R. Briddon[3]

[1]*Departamento de Física, I3N, Universidade de Aveiro, Campus Universitário de Santiago, PT-3810-193 Aveiro, Portugal*

[2]*Department of Physics and Astronomy, Aarhus University, Aarhus, Denmark*

[3]*School of Electrical, Electronic and Computer Engineering, University of Newcastle upon Tyne, Newcastle upon Tyne NE1 7RU, United Kingdom*

(Received 23 July 2011; published 25 October 2011)

Photoluminescence (PL) measurements, performed in Si and $Si_{1-x}Ge_x$ alloys ($x = 0.0069$ and 0.0125) irradiated with protons and annealed between 100 and 650 °C, are combined with first-principles calculations to assess the assignment of the *W* and *X* lines to the trigonal and tetragonal forms of the tri- and tetra-interstitial defects, denoted I_3 and I_4, respectively. It is found that for the *W* line the annealing temperature that maximizes the PL intensity is independent of *x*, whereas for the *X* line a ∼50 °C shift to higher temperatures was observed in the alloys when compared to pure Si. Analysis of the PL quenching mechanisms along with the calculations show that the radiative excited state for both defects comprises a pseudodonor state, where a trapped exciton combines a tightly bound hole and a diffuse electron. The broadening rate as a function of *x* for the *X* line is greater than that of the *W* line by about a factor of two. This is consistent with a stronger electronic localization in the *X* center than in the *W* center, as well as with the relative positions of the donor levels as obtained from the calculations for the I_3 and I_4 defects, respectively. The calculated change rates of donor levels with *x* are in qualitative agreement with the hole binding energy shifts obtained from the experiments. Our results support the assignment of I_3 and I_4 to the *W* and *X* centers, respectively.

DOI: 10.1103/PhysRevB.84.165211 PACS number(s): 61.72.jj, 61.82.Fk, 71.15.Mb, 71.55.Cn

I. INTRODUCTION

Ion implantation and subsequent thermal annealing are key steps in silicon microelectronics industry. Si interstitials created upon implantation are prone to cluster into small and extended defects during post implantation annealing.[1–3] Several Si interstitial related defects have been detected in ion-implanted Si by photoluminescence (PL) spectroscopy.[4–8] These defects are clusters involving different numbers of Si interstitials ranging from small clusters to chains of interstitials and rodlike {311} extended defects, depending on the implantation parameters and subsequent annealing temperature. Among these, the *W* center is present in ion-implanted[9,10] as well as in electron- and neutron-irradiated Si, showing a zero-phonon emission at 1018 meV denoted *W* line.[11,12] The *W* line PL intensity is maximized after annealing in the range 200–250 °C and vanishes upon annealing at ∼500 °C.[13–15] As the *W* line intensity diminishes in PL spectra, another prominent signal with a zero-phonon line (ZPL) at 1040 meV and denoted as *X* line, raises and reaches maximum intensity after annealing in the range 400–500 °C.[14–16]

The recent demonstration of a silicon light-emitting diode[17] based on the *W* center emission is renewing the interest on the structure and formation mechanism of this defect. Moreover, small clusters of Si interstitials, like *W* and *X* centers, play a major role during the initial stages of Si interstitial evolution upon annealing of ion-implanted and irradiated Si. It is also known that such small aggregates are highly mobile at room temperature,[18,19] and lead to transient enhanced diffusion (TED) and deactivation of *p*-type dopants during post-implant anneals.[2,20–26]

Dilute silicon-germanium (SiGe) alloys allow tailoring many properties of otherwise perfect Si or Ge crystals, being simultaneously compatible with the conventional Si complementary metal oxide semiconductor (CMOS) technology.[27] This includes the variation of the energy band gap, mobility, and effective mass of charge carriers. SiGe alloys are particularly well suited for operating at cryogenic temperatures and under radiation-harsh conditions typically found in space exploration.[28] In this kind of environment, radiation defects, including small clusters of Si interstitials, play a critical role in device performance. For instance, a retardation of TED of boron has been observed in SiGe, favoring device downscaling.[29,30] A strong influence of the Ge content on the evolution of Si interstitial clusters has also been reported.[3] For SiGe alloys with Ge content $\leqslant 5\%$, the formation and dissolution of rodlike {311} defects was observed, whereas only dislocation loops were formed if the Ge content was $\geqslant 25\%$.[3] The observation of the *W* and *X* lines in dilute SiGe has been described only in a few reports, and little is known about the influence of minority Ge atoms on the properties of these centers.[16,31] The *W* center emission intensity and line width were found to decrease and increase, respectively, with increasing Ge content.[31] Additionally, its annealing behavior was found to be similar to that of {311} interstitial aggregates.[31]

It is widely accepted that the *W* and *X* centers are of intrinsic nature.[32–34] From uniaxial stress measurements, it has been established that the *W* and the *X* centers possess trigonal and tetragonal symmetry, respectively, with considerably higher stress parameters observed for the *X* center when compared to those of the *W* center.[8,13,32,35] Based on a wide range of spectroscopic data and first-principles calculations, the *W* and *X* centers were assigned to trigonal and tetragonal forms of tri- and tetra-interstitial defects, denoted hereafter by I_3 and I_4, respectively.[8,32,34,36] Structures for these clusters are shown in Fig. 1. While I_3 results from replacement of three

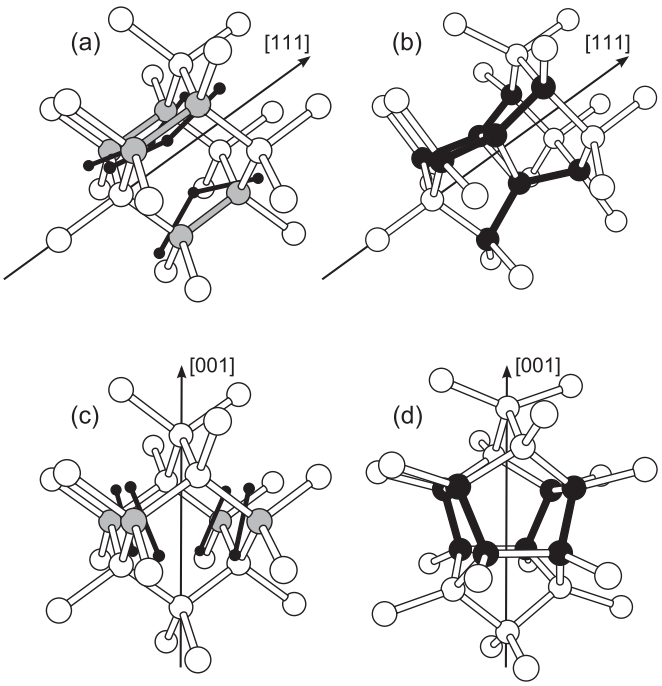

FIG. 1. Atomic models of tri- and tetra-interstitial clusters in Si. (a) and (c) depict a bulklike region of Si atoms (large white and grey balls) for easier understanding of I_3 and I_4 complexes in (b) and (d). In (a), three Si dimers (large grey balls) are replaced by three Si trimers (small black balls) to produce the I_3 cluster shown in (b). In (c), four Si atoms (large grey balls) are replaced by four Si dimers (small black balls) to produce the I_4 complex shown in (d). Note that in both models, all Si atoms are fourfold coordinated.

parallel Si dimers by three ⟨111⟩ aligned Si trimer units, the model of I_4 is obtained by replacing four Si atoms by four Si dimers approximately aligned along the ⟨001⟩.

Arguments supporting the assignment of I_4 [as shown in Fig. 1(d)] to the *X* center are strong and connected with previous theoretical and experimental reports based on techniques other than PL.[36] For instance, it is consensual that the *X* line complex also gives rise to an electron paramagnetic resonance (EPR) center known as B3.[36,37] This is a spin-1/2 signal from a positively charged self-interstitial cluster.[38] The hyperfine structure of B3 shows a tetragonal (D_{2d}) symmetry, like the I_4 center, and the annealing behavior is similar to that observed for the *X* line.[38–40] We note that these observations imply that the B3 center (to be linked with I_4) has a donor level, hereafter denoted $E(0/+)$, within the gap. Moreover, three phonon replicas of the *X* line have been detected both in ^{nat}Si and ^{30}Si enriched samples, demonstrating that the defect has local vibrational modes above the Raman edge.[33] This is characteristic of strongly compressed Si-Si bonds that take place on interstitial defects. These vibrational modes are very close to the highest frequency modes of I_4 that were obtained from previous first-principles calculations.[41]

In contrast, the assignment of the *W* center to I_3 is rather controversial. One of the major arguments behind this connection is the fact that the *W* center is stable at temperatures up to 300 °C, above which the *X* center starts to develop. A single phonon replica of the *W* center ZPL was detected at 70.0 meV, and this shows that the defect has a localized phonon mode above the Raman edge. The replica redshifts by 2.3 meV in heavier ^{30}Si enriched samples, which is consistent with the expected frequency change of a Si-only related mode.[32,33] Like for I_4, this is suggestive of a center with Si-Si bonds under compressive stress. Although the I_3 model shown in Fig. 1(b) accounts for many of the experimentally observed properties of the *W* center,[34,41] recent first-principles modeling of several tri-interstitial configurations, including I_3 from Fig. 1(b), showed that this configuration is energetically disfavored, challenging the assignment of I_3 to the *W* center.[42] Moreover, it is now believed that the I_3 model from Fig. 1(b) is metastable by about 1.6 eV with respect to the ground state.[37,41] According to Estreicher and co-workers, the most stable structure for a tri-interstitial defect in Si possesses C_2 symmetry,[37] and this is incompatible with the trigonal symmetry of the *W* center. Unlike I_4, the tri-interstitial ground state does not induce electronic levels within the Si band gap, meaning that it is not able to hold extra electrons or holes under thermodynamic equilibrium conditions.[37,41] This seems incompatible with a connection to the *W* center as its ZPL energy (1018 meV) implies a stronger exciton localization energy than the *X* center ZPL (1040 meV).

In order to better understand the *W* and *X* lines and their models assignment, we carried out a study of the *W* and *X* centers PL emission properties (line intensity, position, and broadening) as a function of the temperature of post-irradiation annealings and Ge content in dilute $Si_{1-x}Ge_x$ alloys ($x = 0$, 0.0069, 0.0125) irradiated with protons. The data is compared to density functional calculations carried out for the I_3 and I_4 defect structures shown in Figs. 1(b) and 1(d). The energy level schemes of nonradiative de-excitation channels and the influence of the Ge content on the ionization energies of the I_3 and I_4 defects are discussed.

This article is organized as follows. In Sec. II, the experimental details of sample growth, treatments, and measurements are given and in Sec. III, the PL data of *W* and *X* lines are presented and discussed. The theoretical method for the first-principles calculations is presented in Sec. IV, followed by the results on the defect formation and ionization energies in Sec. V. Finally, the conclusions are presented in Sec. VI.

II. EXPERIMENTAL DETAILS

A pure Si layer (denoted S layer) and two dilute $Si_{1-x}Ge_x$ layers with $x = 0.0069$ and 0.0125 (denoted SG1 and SG2 layers, respectively) with 3 μm thickness were grown at 800 °C on Si(001) substrates by means of molecular beam epitaxy (MBE). The Ge content in the layers was determined by Rutherford backscattering spectroscopy (RBS) using 1.5 MeV He^+ ions. Layers SG1 and SG2 were *n*-type doped with Sb. The concentration of conduction electrons measured by the capacitance-voltage technique amounted to 9×10^{15} cm^{-3} and 3×10^{15} cm^{-3} for SG1 and SG2 layers, respectively. Since the contamination resulting from unwanted compensating acceptors should be lower than $\sim 10^{13}$ cm^{-3}, those values should roughly correspond to the concentration of Sb donor atoms in the layers. An *n*-type doping of about 3×10^{14} cm^{-3} resulted from Sb contamination within the growth chamber for the S layer.

The formation of both W and X centers in the $Si_{1-x}Ge_x$ layers of our samples requires the use of particles with high enough mass and a careful choice of the irradiation parameters. All samples were irradiated at room temperature with 875 keV protons through a 10-μm-thick Al foil at a dose of 10^{16} H^+ cm^{-2}. The energy of the protons and the Al foil thickness were chosen based on a SRIM calculation[43] in order to obtain a broad profile of the damage (vacancies/interstitials) in the 3-μm-thick SG layers. The SRIM calculations estimate that the profiles of the vacancies/interstitials and hydrogen atoms have maxima of 2×10^{21} cm^{-3} and 1.25×10^{20} cm^{-3}, respectively. These profiles are centered at 2.2 μm below the surface of the three layers and have a full-width-at-half-maximum (FWHM) of about $\sim$1 μm. It is noteworthy that the SRIM calculations were performed for $T = 0$ K, and at room temperature most of the vacancies and interstitials formed during irradiation recombine. In moderately doped Si, only about 1% of the vacancies/interstitials formed upon irradiation should remain in the sample at room temperature in the form of larger complexes.[44] Therefore, we estimate a maximum concentration profile of vacancies/interstitials after the room-temperature irradiation of about 2×10^{19} cm^{-3}, which is considerably lower than the maximum concentration profile of hydrogen atoms (1.25×10^{20} cm^{-3}). This means that the maximum concentrations of vacancies, interstitials, and hydrogen atoms produced by the irradiations are several orders of magnitude higher than the concentration of Sb donors. After irradiation the samples were annealed for 15 min in a N_2 atmosphere at temperatures between 100 and 650 °C.

The PL measurements were carried out using a Bruker IFS 66v Fourier transform infrared (FTIR) spectrometer equipped with a Ge diode detector. The samples were inserted in a helium gas flow cryostat that allowed to change the temperature in the range 4–300 K. The excitation source was a 488-nm line of an Ar^+ ion laser at a laser power of 13 or 33 mW measured at the front of the cryostat window.

III. PHOTOLUMINESCENCE RESULTS

The PL spectra for the as-irradiated S and SG layers are shown in the top row of Fig. 2. After proton irradiation, only the W line at 1.018 eV is observed in the spectra.

For the layers annealed at 300 °C, the X line starts to emerge in the PL spectrum at $\sim$1.039 eV, in accordance with previous studies.[14,15] The dependence of the W and X line intensities on the annealing temperature (250–600 °C) is shown for all layers in Fig. 3. The annealing temperature that maximizes the PL intensity of the W line is independent of the Ge content. The PL intensity reaches a maximum at 300 °C, decreases for higher values, and almost disappears above 450 °C (see also the middle and bottom rows of Fig. 2). The annealing temperatures that maximize the PL intensity of the X line in the S and SG layers are 400 and 450 °C, respectively. This observation suggests that minority Ge atoms delay the formation of the X center, perhaps by forming intermediate self-interstitial-Ge complexes, or simply by increasing the effective diffusion path length of its precursors.[45] This is compatible with a previous observation where the evolution of interstitial-related defects is influenced by the Ge content in the alloys.[3]

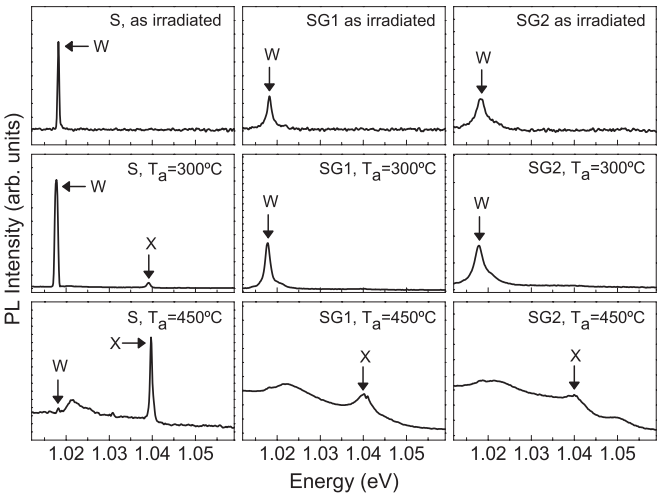

FIG. 2. PL spectra recorded at 5 K for the S, SG1, and SG2 layers as irradiated (top row), after an annealing at $T_a = 300$ °C (middle row), and after annealing at $T_a = 450$ °C (bottom row). All samples were annealed during 15 mins in a N_2 atmosphere. Both W and X lines are identified in the spectra.

With the increase of the Ge content, no shift of the W and X line peak positions is observed in the spectra. For the W line, the FWHM increases at a rate of $d(\text{FWHM})/dx = 229 \pm 48$ meV, which is close to that of 191 meV obtained by Tan *et al.*[31] For the X line, a broadening is also observed with increasing x at a rate of $d(\text{FWHM})/dx = 543 \pm 134$ meV, and clearly higher than that exhibited by the W line. The stronger broadening observed for the X line could be related to a higher localization of the defect wave function on the X center (at the ground or excited state) as compared to the W center. If the effective radius of the wave function is much larger than the interatomic distance, as for the less bound particle in these centers, the change in the number of Ge atoms in the neighborhood is less important. Therefore, the most bound particle in the centers dominates the broadening

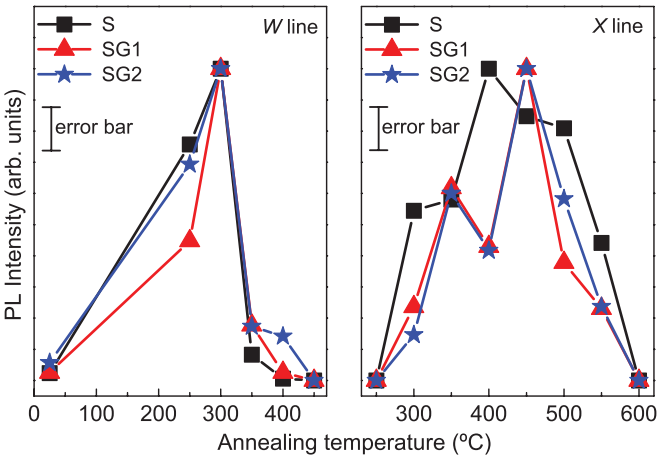

FIG. 3. (Color online) X and W line intensity dependence on the annealing temperature taken at 5 K and for a laser power of 33 mW, for the proton irradiated S (squares), SG1 (triangles), and SG2 (stars) layers. All intensities were normalized to their maximum value. Lines connecting data points are a guide to the eye.

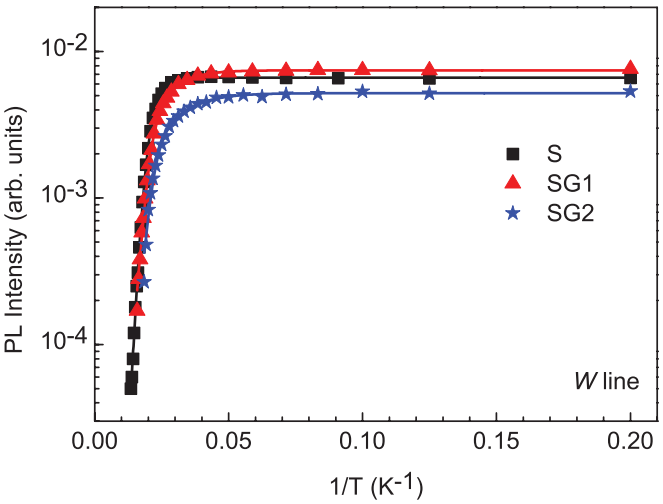

FIG. 4. (Color online) Integrated PL intensity dependence of the W line in S (squares), SG1 (triangles), and SG2 (stars) layers annealed at 300 °C. The data points were used to fit Eq. (1) (shown as solid lines) using the fitting parameters given in Table I.

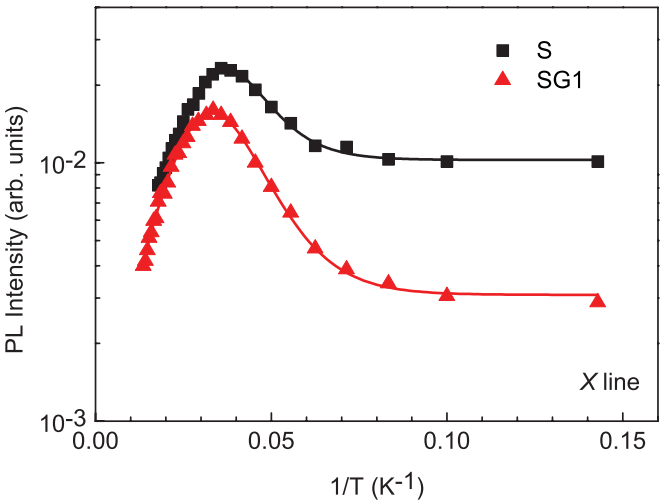

FIG. 5. (Color online) Integral PL intensity dependence of the X line in the S layer annealed at 400 °C (squares), and in the SG1 layer annealed at 450 °C (triangles), together with Eq. (1) (solid lines) using the fitting parameters given in Table I.

behavior. As we shall see, this is consistent with our experimental and theoretical results.

We have monitored the PL intensity as a function of sample temperature to understand the influence of the Ge content on the activation of nonradiative de-excitation mechanisms associated with the W and X centers. In these experiments, all layers were annealed at the temperatures that maximize the intensity of W and X lines. For studying the W line, S and SG layers were all annealed at 300 °C whereas for studying the X line, S and SG layers were annealed at 400 and 450 °C, respectively. The Arrhenius plots for the temperature dependence of the PL intensity of the W line are shown in Fig. 4. As the temperature increases in the range $5 \leqslant T \lesssim 30$ K, we observe a small decrease of the PL intensity. For higher temperatures a strong PL quenching is observed. The temperature dependence of the X line intensity is shown in Fig. 5. Due to strong line broadening effects, this study was not possible for the SG2 layer (see Fig. 2). As shown in Fig. 5, the PL intensity is enhanced with increasing T in the range $5 \leqslant T \lesssim 30$ K, followed by a strong quenching for higher temperatures. However, before proceeding with a more comprehensive analysis of the data, let us generally describe the origin of PL recombination on defects and put forward some premisses.

As will become clear ahead, we consider the hypothesis that without illumination, the defects (D) scrutinized in this work are isoelectronic, neutrally charged, and possess a donor level (hole trap), E_h above the valence band top. A consequence of such a premise is that the character of the hole in the bound exciton state is much like that in the ionized center, whereas the electron is delocalized around the positive core with a weak binding energy E_{bx}.

Under continuous photoexcitation, a steady-state density of free electrons and holes as well as free excitons are generated, and these may be captured at defect radiative states. Radiative recombination related to such electronic states has been previously discussed in the literature.[46–54] The promotion of a defect to an excited state is a requirement for the observation of PL emission. In the model of bound excitons,[46–54] a neutral defect binds a carrier, say a hole, due to a defect-induced potential composed of a short-range central-cell potential and a strain field. The hole localization induces an electrostatic potential (attractive to electrons) which is responsible for binding an electron. The Coulomb character of this potential increases with increasing localization of the hole. This long-range Coulomb-like potential is responsible for electronic excited states appearing close to the conduction band, i.e., shallow donorlike states. Defects in this situation are usually termed as pseudodonors and these excited states are nicely described by effective mass theory (EMT). We should mention that the ground state of a pseudodonor is of a different type than the ground state of a true shallow donor. For true shallow donors, the ground state corresponds to a $1s$ hydrogen-like state, whereas for pseudodonors, the ground state (or more precisely the pseudo-ground-state) actually corresponds to a radiative bound exciton state such as $D^0 + \mathrm{bx}$ in Fig. 6.[52,54] Although for such centers the whole exciton localization energy is $E_h + E_{\mathrm{bx}} = E_{\mathrm{g}} - h\nu$, where E_{g} is the band gap energy, the binding energies of the two excitonic particles are strongly asymmetric, and only that of the loose electron (E_{bx}) is directly accessible by measuring the PL quenching as a function of T.[49,51]

Alternatively, a defect can be electrically inert (with no thermodynamic levels within the gap), and still be able to capture a free exciton before radiative recombination occurs. The total localization energy is now $E_{\mathrm{fx}} + E_{\mathrm{bx}} = E_{\mathrm{g}} - h\nu$, where E_{fx} is the free exciton binding energy, and E_{bx} must be the localization energy of the whole exciton to the center. Note that in this case, dissociation proceeds via promotion of the exciton as a whole to the free excitonic band; according to our hypothesis, the potential of the center is not sufficiently attractive to independently hold any of the exciton particles.

Let us go back to our hypothetical PL active donor center. The energy states of such a complex are shown on the left-hand side of Fig. 6, with its neutral ground state (D^0) and four excited states represented as thick solid lines. The

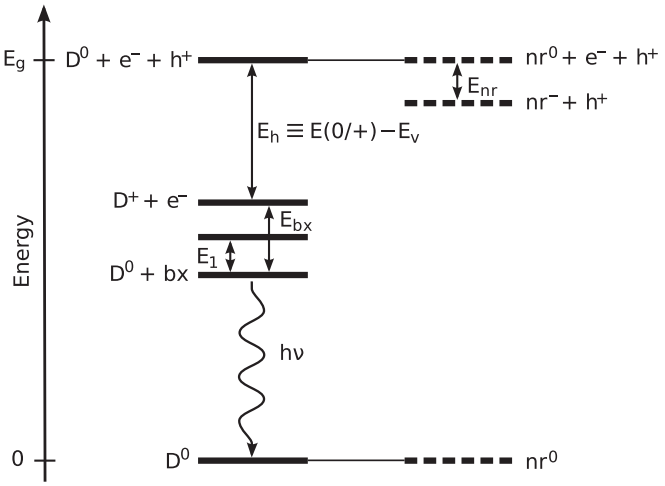

FIG. 6. Energy-level scheme for a PL active center with ZPL energy $h\nu$ and possessing a donor level $E(0/+)$ at the lower half of the gap. The energy to produce an uncorrelated free electron-hole pair ($e^- + h^+$) is the gap width E_g. The radiative excited state is assumed to be made of a tightly bound hole (with binding energy E_h), plus a loose electron with binding energy E_{bx}. Further details of the figure are described in the text.

lowest excited state represents an exciton bound to the defect ($D^0 + \text{bx}$), whereas on upper excited states D^+, e^-, and h^+ denotes the positively charged center, a free electron and a free hole at the conduction band bottom and valence band top, respectively. E_g may be decomposed on the ZPL energy ($h\nu$) and the binding energies of both exciton particles: the hole trap energy (E_h) and the binding energy of the less bound electron E_{bx} (which includes all electron-hole correlation contributions). The state lying E_1 above $D^0 + \text{bx}$ represents a nonradiative excited state of the exciton bound to the defect. It should be noted that for the case of an acceptor center we would be referring to an electron trap (say E_e deep as opposed to E_h) and a negatively charged center ($D^- + h^+$ instead of $D^+ + e^-$), otherwise the energy-level scheme would be similar. Here, the bound exciton would comprise a delocalized hole around an electron tightly bound to the center.

The set of levels shown on the right-hand side of Fig. 6 refers to an effective non-radiative (nr) shallow trap that can release carriers or excitons (that were previously frozen) upon raising the temperature that will be available for capture at D^0. In Fig. 6, this is represented as an electron trap, although it could have been assumed a hole or an exciton trap. Actually, the relevant quantity to explain the observations is solely the activation energy E_{nr} for releasing the carriers or excitons.

The density of centers at the $D^0 + \text{bx}$ radiative state and the sample temperature strongly affect the PL intensity, I. In general, the dependence of I on the temperature can be modeled by the equation[13,55]

$$I(T) = I_0 \left\{ \left[1 + \sum_i c_i \exp\left(-\frac{E_i}{kT}\right) + c_{bx} T^{\frac{3}{2}} \times \exp\left(-\frac{E_{bx}}{kT}\right) \right] \left[1 + \frac{g}{1 + c_{nr} T^{\frac{3}{2}} \exp\left(-\frac{E_{nr}}{kT}\right)} \right] \right\}^{-1}, \quad (1)$$

which is based on the energy-level scheme shown in Fig. 6. In this equation, k is the Boltzmann constant and I_0 is a parameter related to the PL intensity at 0 K, $I(0) = I_0/(1 + g)$, where g accounts for the temperature-independent ratio between the carrier trapping cross section at the radiative defects and at competing shallow traps (nr traps in Fig. 6) described above.

The second and third terms within the first square-bracketed expression accounts for two different PL quenching type channels. One represents the promotion of the loose electron up to a series of discrete excited states of the center each one lying E_i above $D^0 + \text{bx}$ (only one of these states is represented in Fig. 6). The third term accounts for the relative population between the ionized center ($D^+ + e^-$) and the radiative bound exciton state ($D^0 + \text{bx}$), where the electron is freed up to the conduction band and the hole stays trapped at the center.[13,55] The energy E_{bx} refers to the binding energy of the less bound particle of the exciton (the electron), c_i is a parameter proportional to the ratio between the degeneracy of the respective excited state and the $D^0 + \text{bx}$ radiative state, whereas $c_{bx} T^{\frac{3}{2}}$ accounts for the conduction band effective density of states and c_{bx} is a fitting parameter.

The expression within the right-most square brackets describes the thermal supply of "frozen" excitations from traps shallower that E_{bx}, where E_{nr} has been described already. The term $c_{nr} T^{\frac{3}{2}}$ accounts for the effective density of sates of the conduction band, where c_{nr} is a fitting parameter.

Figures 4 and 5 show that the PL intensity of W and X lines display quite different behavior as a function of temperature. Several models were tested in order to fit Eq. (1) to the experimental data. The relevant parameters (and respective uncertainties) of the best fits for both centers are presented in Table I. For the W line, the best results were obtained by considering both PL quenching channels described above and depicted in Fig. 6: (i) thermal excitation of the center to an effective discrete and nonradiative excited state located at an energy of E_1 above the radiative state and (ii) thermal dissociation of the exciton upon ionization of the electron to the conduction band. This state lies E_{bx} above the radiative state and $E_{bx} > E_1$. The first mechanism is responsible for the small decrease of the intensity in the range $5 \leqslant T \lesssim 30$ K,

TABLE I. Energies and respective uncertainties, in meV, obtained from the fit of Eq. (1) to the data related to the temperature dependence of the intensity of the W and X lines measured for the S, SG1, and SG2 layers. The binding energies E_{bx} obtained for the W line in Si by Giri[8] and Yang[56] are shown for comparison. The hole trap depth was estimated by assuming the variation of E_g with the Ge content as reported in Ref. 58.

Center	Layer	E_{nr}	E_1	E_{bx}	E_h
W	S	...	28 ± 2	65 ± 6	87 ± 9
		...	...	59[a]	...
		...	...	50[b]	...
	SG1	...	11.7 ± 0.8	43 ± 3	106 ± 7
	SG2	...	9 ± 1	40 ± 6	106 ± 9
X	S	11 ± 1	...	14 ± 1	116 ± 7
	SG1	8.4 ± 0.7	...	12.5 ± 0.8	114 ± 7

[a]Reference 8.
[b]Reference 56.

whereas the strong PL quenching for higher temperatures is dominated by the second mechanism. For the first channel, activation energies E_1 of 28 ± 2, 11.7 ± 0.8, and 9 ± 1 meV were obtained for the S, SG1, and SG2 layers, respectively. For the thermal ionization energies (E_{bx}), values of 65 ± 6, 43 ± 3, and 40 ± 6 meV were obtained for the S, SG1, and SG2 layers, respectively. The E_{bx} value obtained for the S layer is close to that reported by other authors[8,56] for the same center in Si^+ implanted Si. Davies *et al.*[32] also observed a strong quenching of the W line in the range 10–50 K in neutron irradiated Si, although an activation energy has not been extracted from their data.

In the case of the X line (Fig. 5), the best fit to the data was obtained by considering the thermal ionization quenching mechanism balanced by the binding energy E_{bx}, and a feeding mechanism due to existing shallow traps parameterized by the activation energy E_{nr}. The first mechanism leads to the observed PL quenching at higher T, whereas the latter mechanism is responsible for the raise in PL intensity observed with increasing T in the low-temperature range. For the thermal ionization energies E_{bx}, we obtained values of 14 ± 1 and 12.5 ± 0.8 meV for the S and SG1 layers, respectively, while for the depth of the nonradiative shallow traps, E_{nr}, we found 11 ± 1 and 8.4 ± 0.7 meV for the S and SG1 layers, respectively (see Table I). The increase of PL in the low-temperature range was not observed for the W line. Such an effect could be explained by the fact that W and X line intensity measurements were made on samples previously annealed at different temperatures. This may have an impact on the type and concentration of shallow traps that are formed under such conditions.

Up to this point, our analysis was based on the assumption that the observed thermal quenching of the PL for the W and X lines involved the promotion of a carrier less bound to the center (hypothesized to be the electron) to an excited state, and that the defects are electrically active. However, one could argue that the PL quenching results from exciton release as a whole (see Ref. 51 for further details). As already pointed out, for such centers, the binding energy of the exciton E_{bx} is the difference between the excitonic gap $E_g^{ex} = E_g - E_{fx} = 1.1547$ eV (Ref. 57) and the energy of the radiative transition $h\nu$. This gives $\sim$0.137 eV and $\sim$0.116 eV for the W and X lines, respectively. These values are considerably larger than the E_{bx} energies obtained experimentally (see Table I), and this discrepancy clearly supports the premisse previously assumed, i.e., the thermal quenching of the PL originates from the release of the less-bound carrier, hence leaving the center on a charged state.

The localization energy of the hole as a function of Ge content can be estimated as $E_h(x) = E_g(x) - E_{bx}(x) - h\nu(x)$. To first order, the excitonic band gap in Si-rich SiGe alloys was measured as $E_g^{ex}(x) = 1.155 - 0.43\,x$ eV.[58] We assume that the change of the uncorrelated electron-hole pair energy gap with x, dE_g/dx, is identical to that of dE_g^{ex}/dx. Such an assumption derives from the fact that the free-exciton binding energy changes by about $dE_{fx}/dx \approx -0.01$ eV if we consider a linear change from $E_{fx} = 14.7$ meV in Si to $E_{fx} = 4.18$ meV in Ge.[59,60] Values of E_h obtained from the measured data are reported in Table I. They indicate that in pure Si layers, W and X centers produce deep carrier traps at 87 and 116 meV, respectively, away from one of the band edges. From Ref. 58, the error of the measured gap in the alloy $\Delta E_g^{ex} \approx \Delta E_g$ is approximately 7 meV. Combining this figure with the E_{bx} uncertainties we may estimate the error bars for E_h reported in Table I.

It is also interesting to note that for both W and X centers, we observe a decrease of the ionization energy E_{bx} with increasing Ge content. This suggests an increasingly delocalized state of the loose particle due to increase of the electronic screening of the alloy (as compared to pure Si). Moreover, E_{bx} values are lower for the X center than for the W center, i.e., the asymmetry in the binding energies of the excitonic particles is more pronounced in the X center than in the W center.

IV. THEORETICAL METHOD

In order to link the experimental observations to defect structures, we investigated the two interstitial models shown in Fig. 1, and previously proposed for the W and X centers in SiGe alloys. The defects were modeled within the framework of density-functional theory. Core electrons were dealt with by using the pseudopotentials proposed by Hartwigsen, Goedecker, and Hutter (HGH).[61] We adopted the local density approximation (LDA) for the exchange and correlation energy, together with an expansion of the Kohn-Sham states in a basis set of localized Cartesian Gaussian orbitals (CGOs), as implemented in the AIMPRO code.[62] For Si, we used a contracted basis set with polarization functions to account for higher-order momentum components, with a total of 13 functions per atom (44G*). Basis set production details and convergence tests for Si have been reported elsewhere.[63] The geometry, relative energies, and electronic levels of I_3 and I_4 defects in Si calculated using this methodology are in close agreement with those that we have obtained previously using a combination of uncontracted basis sets with 22 and 28 functions per atom.[41] For example, E_h values previously obtained for both defects differ by less that 0.01 eV when compared to the present calculations. For Ge, we used an uncontracted basis set of (4,4,2) (s,p,d) CGOs, with a total of 28 functions per atom.

Defects were placed in 216 atom cubic supercells, and the Brillouin zone was sampled with the help of 2^3 special **k** points as proposed by Monkhorst and Pack.[64] The alloy was modeled by generating a series of random $Si_{216-n}Ge_n$ supercells. In accordance with the layers studied in PL in this work, the theoretical study was restricted to Ge concentrations below 2.5% which corresponds in average to values of n between zero and five. For each n, we generated twenty SiGe supercells by placing the Ge atoms at random sites of the silicon lattice. In previous work, it was shown that the calculated lattice parameters reproduce well the structural properties of the alloys over all the concentration range,[65,66] and that for the small concentrations that are relevant for this work, Vegard's law[67] is a good approximation.[68,69] Although for comparable Si and Ge concentrations a small bowing of the the lattice parameter (a_0) is observed,[65] the lattice parameter for our SiGe supercells was obtained by linear interpolation between a_0 values for bulk Si and bulk Ge.

In the following section, we compare the electronic structure of I_3 and I_4 in SiGe alloys, with the experimental results reported in Sec. III.

V. MODELING RESULTS

A. Defect structure and formation energy

The structure and stability of I_3 and I_4 in Si have been described in a previous paper.[41] While I_4 is a very stable defect with only one known low-formation-energy configuration, the tri-interstitial ground state is very mobile[37] and the I_3 form depicted in Fig. 1(b), which has been linked to the *W* center, is at least 1.6 eV higher in energy than the most stable configuration.[37,41]

The energy shift of exciton recombination at a donor center in SiGe alloys comprises the variation of the band gap (E_g), the hole binding energy (E_h), and the electron binding energy (E_{bx}) as shown in Fig. 6. These quantities depend on (i) short-range effects when at least one of the electronic states involved in the transition overlap one or more minority alloying species and (ii) long-range effects like the change of the dielectric screening or elasticity of the SiGe host matrix.

Short-range interactions, will drive the formation of I_3 and I_4 defects with a preference for Si core atoms. Both interstitial aggregates produce a compressive strain on surrounding Si-Si bonds. Our results indicate that in Si, bonds at the core of I_3 and I_4 are shortened by 15.5 and 10.4% with respect to the bulk value, respectively. Thus, the larger Ge atoms avoid the compressive stress field produced by the interstitial defects. This results in negative binding energies (higher than -0.11 and -0.20 eV for I_3 and I_4, respectively).

Long-range effects were investigated by generating a series of twenty $Si_{216-n}Ge_n$:*D* supercells, where *D* stands for I_3 or I_4, with a total of 216 + 3 or 216 + 4 atoms, respectively. In order to isolate the long-range effect of the alloy, Ge atoms were not placed in the immediate neighborhood to the defects. After all, this is consistent with the lower formation energies of these aggregates, i.e., when Ge atoms are at remote locations. Ge substitution was assumed to be equally probable on all remaining lattice positions. For each supercell, the positions of all atoms were relaxed at a fixed volume (using Vergad's linear relation), assuming the respective Ge content *x*.

Defect formation energies are given by

$$E_{f,D}(x) = E_D(x) - E_{bulk}(x) - m\mu_{Si}, \tag{2}$$

where $E_D(x)$ is the average energy of the defective supercells with a Ge content *x*, $E_{bulk}(x)$ is the average energy of the bulk SiGe supercells for the same *x*, *m* is the number of self-interstitials and μ_{Si} is the chemical potential of Si.

The calculated formation energies, obtained with μ_{Si} taken from bulk Si, are shown in Fig. 7. The formation energy per atom is higher for I_3 than for I_4 both in Si and in the alloys. In both cases, $E_{f,D}(x)$ decreases with *x*. This can be explained by the larger lattice constant and lower cohesive energy with higher the Ge content. However, the variation in the formation energy with *x* is very small, amounting to less than 2% for both defects for the concentrations considered.

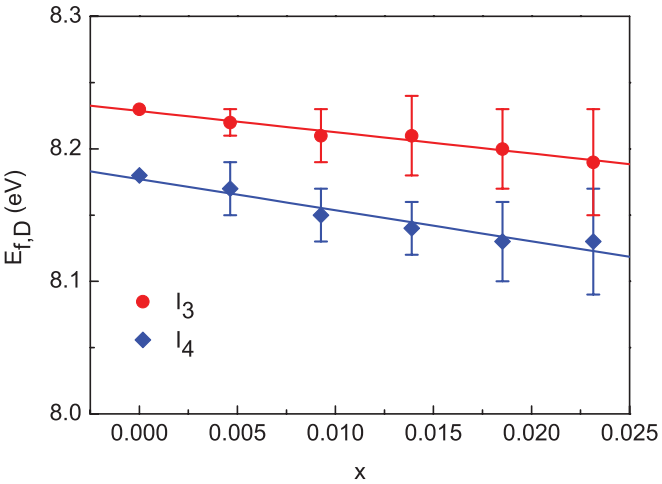

FIG. 7. (Color online) Calculated formation energies of I_4 and I_3 in $Si_{1-x}Ge_x$ alloys. μ_{Si} was taken from bulk Si. Error bars represent the statistical standard deviation of $E_{f,D}$ for the configurations sampled.

B. Ionization levels

The ionization potential, given relative to an arbitrary reference, can be obtained from the absolute difference between the total energies of supercells containing the defect *D* in the neutral and positive charge states,

$$\phi_D(0/+) = E_{D^0} - E_{D^+}. \tag{3}$$

Similarly, electron affinities can be obtained from the difference between the total energies of negatively charged and neutral supercells,

$$\phi_D(-/0) = E_{D^-} - E_{D^0}. \tag{4}$$

The energy $E_h = E(0/+) - E_v$ corresponding to the position of the donor level with respect to the valence band top (see Fig. 6), can be calculated by comparing the ionization potential of the defect with the ionization potential of a bulk (*B*) supercell:

$$E(0/+) - E_v = \phi_D(0/+) - \phi_B(0/+), \tag{5}$$

This is equivalent to the marker method, using the bulk solid host as marker.[63] The position of acceptor levels with respect to the conduction band bottom can be found using the same method, as

$$E_c - E(-/0) = \phi_B(-/0) - \phi_D(-/0). \tag{6}$$

In pure Si supercells, we find that both I_3 and I_4 are donors with levels at $E_h = 0.18$ and 0.29 eV, respectively. No acceptor level in the gap was found for either of them. These figures are consistent with our hypothesis according to which both *W* and *X* centers possess a tightly bound hole in their excited radiative states. Additionally, this is consistent with the assignment of *W* and *X* center to I_3 and I_4, respectively, due to the fact that E_h is lower for the *W* center.

The marker method can be applied across a concentration range *x*, yielding the shift of defect levels with the Ge

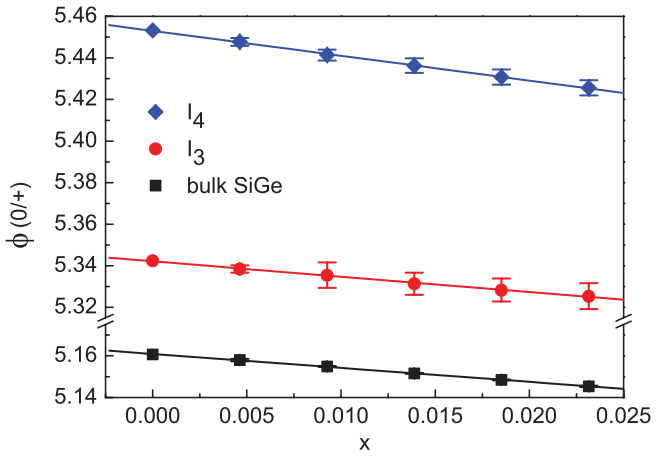

FIG. 8. (Color online) Calculated ionization energies of I_3, I_4, and bulk SiGe alloys as a function of the Ge content, x, using Si_nGe_{216-n} supercells.

content.[70] Since, as detailed in Sec. I, the assignment of the X center to I_4 has been rather firmly established, let us start by comparing the theoretical and experimental results for this defect. The relevant ionization potentials as a function of x, are shown in Fig. 8. The values of $\phi(0/+)$ for bulk (squares) should be taken as the valence band top of the alloy. All uncertainties (shown as error bars) represent the standard deviations of the total energies for the configurations sampled. These should be taken with care as they are considerably lower than the usual overall error of the marker method of the order of 0.1 eV (estimated by comparing several calculated level positions with experimental data for defects in group-IV semiconductors).[63]

The shift of the donor level with the Ge content can be determined using Eqs. (3) and (5). For I_4, we obtain $E_h = 0.29 - (0.52 \pm 0.02)x$ eV. Hence, the distance from the $E(0/+)$ level to the top of the valence band decreases with x. Since the Ge atoms can be viewed as a small perturbation to the system, we expect the $dE(0/+)/dx$ rate to be more accurate than the individual $E(0/+)$ values. Experimentally, this rate is difficult to determine. From the E_h values in Table I, we obtain $dE(0/+)/dx \backsimeq \Delta E_h/\Delta x = -0.29$ eV where ΔE_h and Δx are differences between respective values. This figure is in qualitative agreement with the one obtained from theory (-0.52), but since the calculated E_h value and its error are of the same order of magnitude, we cannot establish a quantitative comparison.

For the I_3 model, we obtain $E_h = 0.18 - (0.07 \pm 0.02)x$. In contrast with I_4, in this case the $E(0/+)$ remains practically parallel to the valence band top, suggesting that the hole state has a strong valence-band character. The experimental values in Table I suggest that the E_h of the W line increases with x, with $\Delta E_h/\Delta x$ between 1.5 and 2.8 eV. However, if we consider the error associated to the experimental values of E_h, the above values for $\Delta E_h/\Delta x$ can vary by more than one order of magnitude. Thus, this comparison of the theory with the experimental data is not necessarily in contradiction with the assignment of the W line to the I_3. Therefore further work is necessary to establish a reliable comparison between experiments and theory.

VI. DISCUSSION AND CONCLUSIONS

An investigation of optical properties and thermal stability of the W and X lines in Si and SiGe alloys with low Ge content ($x = 0.0069$ and 0.0125), was presented along with density functional calculations of the electronic structure of I_3 and I_4 self-interstitial aggregates in dilute SiGe supercells. The comparison of experimental and theoretical results supports the assignment of I_3 and I_4 to the W and X centers, respectively.

The defects were produced by proton irradiation and the PL intensity of the W line was found to attain a maximum value after an annealing at 300 °C, independently of the Ge content in the SiGe alloy. On the other hand, for the X line, the presence of Ge shifted the above annealing temperature from 400 °C in pure Si to 450 °C in SiGe alloy. No shift of the W and X line peak positions is observed in the spectra with the increase of the Ge content. However, the FWHM broadening rates [d(FWHM)$/dx$] of the two lines are quite different, namely 229 ± 48 meV for the W line and 543 ± 134 meV for the X line, which is interpreted as a difference in the localization of the defect wave function for both centers. Two nonradiative PL quenching channels were identified for the W line. One involves the promotion from the radiative state to a higher energy bound excitonic state, whereas the other, corresponds to the escape of the loose particle to a band. For the X line, only the latter mechanism was identified.

From density functional calculations, a donor level was obtained for both self-interstitial cluster models I_3 and I_4. The donor level of I_3 ($E_v + 0.18$ eV) was found closer to the valence band top than that of I_4 ($E_v + 0.29$ eV). The calculations also find that E_h for I_3 is almost pinned to the valence band edge (as a function of the Ge content x) with a shift rate of $-0.07x$ eV, whereas for I_4, E_h shifts toward the valence band top at a rate of $-0.52x$ eV. These figures are qualitatively in agreement with the experiments. A simple extrapolation suggests that the I_4 defect is not electrically active for $x \gtrsim 0.5$.

Ge minority species act as effective probes to examine the local structure of defects. While the annealing temperature that maximizes the intensity of the W center (which is already present in as-irradiated samples) is not affected by the presence of Ge, the analogous temperature for the X line is increased by about 50 °C. Since I_3 and I_4 are strongly compressive, theory excludes the formation of stable I_3-Ge and I_4-Ge complexes. This is compatible with a picture where the aggregation of diffusing self-interstitial precursors will be hindered by Ge scattering centers that increase the effective activation energy for the formation of larger I_n complexes.

Analysis of the PL quenching data and electrical level calculations allowed us to conclude that the radiative state comprises a trapped exciton where the hole is more tightly bound to the defect than the electron. Accordingly, de-excitation of both centers can be described by the release of a weakly bound electron leaving behind a positively charged center. The asymmetry in the binding energies is higher in the X center than in the W center and it is consistent with the PL line broadening dependence with the Ge content. The depths of the hole traps (E_h) were also estimated from the PL quenching data. These are related to (0/+) levels, and in pure Si they were measured at $E_v + 116$ meV and $E_v + 87$ meV for

the *X* and *W* centers, respectively. This analysis was extended to diluted SiGe alloys, and it allowed us to establish a link with the theoretical donor level calculations for pure Si and alloys with different Ge content.

ACKNOWLEDGMENTS

A.C. is supported by Fundação para a Ciência e Tecnologia (FCT) and the Marie Curie SiNanoTune project.

*joaquim.leitao@ua.pt

[1] K. S. Jones, S. Prussin, and E. R. Weber, Appl. Phys. A **45**, 1 (1988).
[2] S. C. Jain, W. Schoenmaker, R. Lindsay, P. A. Stolk, S. Decoutere, M. Willander, and H. E. Maes, J. Appl. Phys. **91**, 8919 (2002).
[3] R. T. Crosby, K. S. Jones, M. E. Law, A. N. Larsen, and J. L. Hansen, Mater. Sci. Semicond. Process. **6**, 205 (2003).
[4] J. L. Benton, S. Libertino, P. Kringhøj, D. J. Eaglesham, J. M. Poate, and S. Coffa, J. Appl. Phys. **82**, 120 (1997).
[5] D. C. Schmidt, B. G. Svensson, M. Seibt, C. Jagadish, and G. Davies, J. Appl. Phys. **88**, 2309 (2000).
[6] S. Libertino, S. Coffa, and J. L. Benton, Phys. Rev. B **63**, 195206 (2001).
[7] M. Nakamura and S. Murakami, J. Appl. Phys. **94**, 3075 (2003).
[8] P. K. Giri, Semicond. Sci. Technol. **20**, 638 (2005).
[9] J. R. Noonan, C. G. Kirkpatrick, and B. G. Streetman, Radiat. Eff. **21**, 225 (1974).
[10] C. G. Kirkpatrick, J. R. Noonan, and B. G. Streetman, Radiat. Eff. **30**, 97 (1976).
[11] M. Nakamura and S. Nagai, Phys. Rev. B **66**, 155204 (2002).
[12] J. A. Rostworowski and R. R. Parsons, Can. J. Phys. **59**, 496 (1981).
[13] G. Davies, Phys. Rep. **176**, 83 (1989).
[14] K. Terashima, T. Ikarashi, M. Watanabe, and T. Kitano, Mater. Sci. Forum **258-263**, 587 (1997).
[15] O. O. Awadelkarim, A. Henry, B. Monemar, J. L. Lindström, Y. Zhang, and J. W. Corbett, Phys. Rev. B **42**, 5635 (1990).
[16] A. O. Ankiewicz, N. A. Sobolev, J. P. Leitão, M. C. Carmo, R. N. Pereira, J. L. Hansen, and A. N. Larsen, Nucl. Instrum. Methods Phys. Res., Sect. B **248**, 127 (2006).
[17] J. Bao, M. Tabbal, T. Kim, S. Charnvanichborikarn, J. S. Williams, M. J. Aziz, and F. Capasso, Opt. Express **15**, 6727 (2007).
[18] G. D. Watkins, Phys. Rev. B **12**, 5824 (1975).
[19] E. J. H. Collart, K. Weemers, N. E. B. Cowern, J. Politiek, P. H. L. Bancken, J. G. M. van Berkum, and D. J. Gravesteijn, Nucl. Instrum. Methods Phys. Res., Sect. B **139**, 98 (1998).
[20] P. M. Fahey, P. B. Griffin, and J. D. Plummer, Rev. Mod. Phys. **61**, 289 (1989).
[21] N. E. B. Cowern, K. T. F. Janssen, and H. F. F. Jos, J. Appl. Phys. **68**, 6191 (1990).
[22] P. A. Stolk, D. J. Eaglesham, H.-J. Gossmann, and J. M. Poate, Appl. Phys. Lett. **66**, 1370 (1995).
[23] P. A. Stolk, H.-J. Gossmann, D. J. Eaglesham, D. C. Jacobson, C. S. Rafferty, G. H. Gilmer, M. Jaraíz, J. M. Poate, H. S. Luftman, and T. E. Haynes, J. Appl. Phys. **81**, 6031 (1997).
[24] A. Ural, P. B. Griffin, and J. D. Plummer, J. Appl. Phys. **85**, 6440 (1999).
[25] N. E. B. Cowern, G. Mannino, P. A. Stolk, F. Roozeboom, H. G. A. Huizing, J. G. M. van Berkum, F. Cristiano, A. Claverie, and M. Jaraíz, Phys. Rev. Lett. **82**, 4460 (1999).
[26] S. Charnvanichborikarn, B. J. Villis, B. C. Johnson, J. Wong-Leung, J. C. McCallum, J. S. Williams, and C. Jagadish, Appl. Phys. Lett. **96**, 051906 (2010).
[27] F. Schäffler, Semicond. Sci. Technol. **12**, 1515 (1997).
[28] J. D. Cressler, in *Custom Integrated Circuits Conference*, CICC 2008 (IEEE, San Jose, CA, 2008), pp. 57–64.
[29] P. Kuo, J. L. Hoyt, J. F. Gibbons, J. E. Turner, and D. Lefforge, Appl. Phys. Lett. **66**, 580 (1995).
[30] C. C. Wang, Y. M. Sheu, S. Liu, R. Duffy, A. Heringa, N. E. B. Cowern, and P. B. Griffin, Mater. Sci. Eng. B **124-125**, 39 (2005).
[31] J. Tan, G. Davies, S. Hayama, and A. N. Larsen, Appl. Phys. Lett. **90**, 041910 (2007).
[32] G. Davies, E. C. Lightowlers, and Z. E. Ciechanowska, J. Phys. C **20**, 191 (1987).
[33] S. Hayama, G. Davies, and K. M. Itoh, J. Appl. Phys. **96**, 1754 (2004).
[34] B. J. Coomer, J. P. Goss, R. Jones, S. Öberg, and P. R. Briddon, Physica B **273-274**, 505 (1999).
[35] Z. Ciechanowska, G. Davies, and E. C. Lightowlers, Solid State Commun. **49**, 427 (1984).
[36] B. J. Coomer, J. P. Goss, R. Jones, S. Öberg, and P. R. Briddon, J. Phys. Condens. Matter **13**, L1 (2001).
[37] S. K. Estreicher, M. Gharaibeh, P. A. Fedders, and P. Ordejón, Phys. Rev. Lett. **86**, 1247 (2001).
[38] K. L. Brower, Phys. Rev. B **14**, 872 (1976).
[39] T. Mchedlidze and M. Suezawa, J. Phys. Condens. Matter **15**, 3683 (2003).
[40] D. Pierreux and A. Stesmans, Phys. Rev. B **68**, 193208 (2003).
[41] A. Carvalho, R. Jones, J. Coutinho, and P. R. Briddon, Phys. Rev. B **72**, 155208 (2005).
[42] G. M. Lopez and V. Fiorentini, J. Phys. Condens. Matter **15**, 7851 (2003).
[43] J. F. Ziegler, J. P. Biersack, and U. Littmark, *The Stopping and Range of Ions in Solids* (Pergamon, New York, 1985).
[44] A. P. Knights, F. Malik, and P. G. Coleman, Appl. Phys. Lett. **75**, 466 (1999).
[45] A. N. Larsen, A. B. Hansen, D. Reitze, J.-J. Goubet, J. Fage-Pedersen, and A. Mesli, Phys. Rev. B **64**, 233202 (2001).
[46] J. J. Hopfield, in *Proceedings of the Seventh International Conference on the Physics of Semiconductors*, edited by M. Hulin (Dunod Cie & Academic, Paris, 1964), pp. 725–735.
[47] J. J. Hopfield, D. G. Thomas, and R. T. Lynch, Phys. Rev. Lett. **17**, 312 (1966).
[48] P. J. Dean, J. Lumin. **7**, 51 (1973).
[49] M. D. Sturge, E. Cohen, and K. F. Rodgers, Phys. Rev. B **15**, 3169 (1977).
[50] W. Hayes and A. M. Stoneham, *Defects and Defect Processes in Nonmetallic Solids* (Wiley, New York, 1985), p. 273.
[51] R. Sauer and J. Weber, Physica B+C **116**, 195 (1983).
[52] J. H. Svensson, B. Monemar, and E. Janzén, Phys. Rev. Lett. **65**, 1796 (1990).
[53] M. Kleverman, J.-O. Fornell, J. Olajos, H. G. Grimmeiss, and J. L. Lindström, Phys. Rev. B **37**, 10199 (1988).

[54]M. Kleverman, Mater. Sci. Forum **258-263**, 497 (1997).
[55]K. Thonke, J. Weber, J. Wagner, and R. Sauer, Physica B+C **116**, 252 (1983).
[56]Y. Yang, J. Bao, C. Wang, and M. J. Aziz, J. Appl. Phys. **107**, 123109 (2010).
[57]G. S. Mitchard and T. C. McGill, Phys. Rev. B **25**, 5351 (1982).
[58]J. Weber and M. I. Alonso, Phys. Rev. B **40**, 5683 (1989).
[59]N. O. Lipari and M. Altarelli, Phys. Rev. B **15**, 4883 (1977).
[60]M. Altarelli and N. O. Lipari, Phys. Rev. Lett. **36**, 619 (1976).
[61]C. Hartwigsen, S. Goedecker, and J. Hutter, Phys. Rev. B **58**, 3641 (1998).
[62]P. Briddon and R. Jones, Phys. Status Solidi B **217**, 131 (2000).
[63]J. P. Goss, M. J. Shaw, and P. R. Briddon, in *Theory of Defects in Semiconductors*, edited by D. A. Drabold and S. K. Estreicher, Topics in Applied Physics Vol. 104 (Springer, Berlin, 2007), Chap. 3, p. 69.
[64]H. J. Monkhorst and J. D. Pack, Phys. Rev. B **13**, 5188 (1976).
[65]J. P. Dismukes, L. Ekstrom, and R. J. Paff, J. Phys. Chem. **68**, 3021 (1964).
[66]A. Balsas, J. Coutinho, V. J. B. Torres, P. R. Briddon, and M. Barroso, Phys. Rev. B **70**, 085201 (2004).
[67]L. Vegard, Z. Phys. **5**, 17 (1921).
[68]J. C. Aubry, T. Tyliszczak, A. P. Hitchcock, J.-M. Baribeau, and T. E. Jackman, Phys. Rev. B **59**, 12872 (1999).
[69]A. Chroneos, H. Bracht, C. Jiang, B. P. Uberuaga, and R. W. Grimes, Phys. Rev. B **78**, 195201 (2008).
[70]A. Carvalho, J. Coutinho, R. Jones, J. Goss, M. Barroso, and P. R. Briddon, Phys. Rev. B **78**, 125208 (2008).